Tellus (1996), 48A, 193–208
Printed in Belgium – all rights reserved

TELLUS
ISSN 0280–6495

A warm core in a polar low observed with a satellite microwave sounding unit

By JOHN M. FORSYTHE*, *Science and Technology Corporation, Metsat Division, 515 S. Howes St., Fort Collins, Colorado, USA 80521*, and THOMAS H. VONDER HAAR, *Science and Technology Corporation, Metsat Division, and Cooperative Institute for Research in the Atmosphere, Colorado State University, Fort Collins, Colorado, USA 80523*

(Manuscript received 3 November 1994; in final form 5 July 1995)

ABSTRACT

A polar low which occurred over the Labrador Sea on 17 and 18 January 1989 was examined with the Microwave Sounding Unit (MSU) on the satellites NOAA-10 and 11. Surface reports indicated a pressure deficit of at least 4 mb with the polar low, and surface wind speeds of at least 20 m/s were retrieved with the Special Sensor Microwave/Imager. MSU brightness temperatures at 53.74 GHz were warmer over the polar low than in all of the adjacent MSU field-of-views. The 53.74 GHz brightness temperatures over the polar low were between 1 and 2 K warmer than the adjacent values. Since some polar lows are warm core systems, results of this type are expected. The possibility that the warming observed in the 53.74 GHz data was caused by factors other than warming of the air column was investigated. MSU 50.30 GHz brightness temperatures did not show a maximum over the polar low, as would be expected if the 53.74 GHz warming was caused by surface and precipitation effects. A sensitivity analysis indicates that the measured warming is greater than that expected from cloud and surface effects. This type of measurement should be a useful tool for monitoring polar lows, particularly when the higher resolution Advanced Microwave Sounding Unit becomes available.

1. Introduction

Polar lows are subsynoptic-scale cyclones which form poleward of the polar front, often over water adjacent to the ice boundary. Their horizontal scale is on the order of a few hundred kilometers and they can pass through their entire life cycle in a few hours to a couple of days. Winds greater than gale force, heavy snowfall rates, low visibility, and freezing sea spray can make them a dangerous type of storm. Polar lows have only been known as a distinct type of storm for about 25 years and the mechanisms responsible for their genesis and intensification are a topic of current research (e.g., Montgomery and Farrell, 1992). Baroclinic instability, positive feedback of cumulus convection, and air sea interaction instability have all been proposed as having roles in the life of a polar low. Polar lows often occur over remote oceanic regions, where there is frequently a lack of conventional meteorological observations. In fact, the first research aircraft measurements of a polar low were only taken in 1984 (Shapiro et al., 1987). The polar low is a recently enough recognized atmospheric phenomenon that even its definition is somewhat controversial (Rasmussen et al., 1993; Businger and Reed, 1989).

An interesting feature of some polar lows in satellite imagery is their striking similarity to tropical cyclones (Nordeng and Rasmussen, 1992; Rasmussen, 1989). Spiral cloud bands, a cloud free eye, occurrence over water, and deep convection are among the features which have led to this comparison. It should be emphasized that polar lows can exhibit a wide range of cloud structures and there is not a cloud morphology unique to all polar lows (Forbes and Lottes, 1985).

Surface temperatures which are warmest near the center of the polar low have been observed

*Corresponding author

in several case studies (Businger and Baik, 1991; Douglas et al., 1991; Shapiro et al., 1987; Rasmussen, 1985). Several mechanisms have been suggested to explain this warm central region in a polar low, referred to as a warm core. The first is a process called seclusion, where warm ambient air is surrounded and then cut off by colder air flowing around the storm. Another possible method for the production of warm surface temperatures in a polar low is through a flux of sensible and latent heat from the sea surface. The presence of strong sensible and latent heat fluxes in polar lows, up to 1000 W/m^2 or even greater, has been well documented (Rasmussen et al., 1993; Businger and Baik, 1991; Shapiro et al., 1987). This is on the order of the total surface heat flux in a tropical cyclone, although a greater fraction is partitioned into sensible heat flux in polar lows due to the larger ($\sim$5°C) air sea temperature difference which is usually found in the polar low. Production of a warm core through moist adiabatic ascent and dry adiabatic descent of air in a polar low can only make a small contribution to warming in the lowest layers of a polar low (Rasmussen, 1989), due to the low moisture content of the cold air. The question of whether a polar low develops a warm core has implications for whether the storm will fill or deepen (Van Delden, 1989), as well as to whether the strongest winds will occur near the surface or in the upper troposphere.

In this paper, which is an extension of the work of Forsythe (1993), measurements from the Microwave Sounding Unit (MSU), a microwave radiometer which is sensitive to tropospheric temperature and is on board the polar orbiting satellites NOAA 10 and 11, are used to detect an isolated warm core in a polar low. The polar low occurred on 17 and 18 January 1989, in the Labrador Sea, a region which has only recently received attention in polar low studies (Rasmussen and Purdom, 1992). The magnitude of the observed warming will be given, and the possible effects of clouds and the surface in causing warm microwave brightness temperatures will be examined. Applications of microwave temperature sounding instruments in the analysis of polar lows will be discussed.

This application of the MSU to detect warming over a polar low is similar to previous work using this instrument for both tropical and extratropical cyclones. Satellite measurements of the upper tropospheric warming in the tropical cyclone, determined with microwave temperature sounding instruments which use oxygen emission, have been used to empirically estimate storm central pressure deficit and maximum wind speed (Velden et al., 1991; Velden, 1989; Velden and Smith, 1983; Kidder et al., 1980; Kidder et al., 1978). The magnitude of the observed warming over several tropical cyclones ranged up to 5°K of brightness temperature (hereafter referred to as T_B) above the ambient T_B. Brightness temperature is the quantity usually referred to in microwave radiometry since it is nearly linearly proportional to radiance through the Rayleigh-Jeans approximation. Brightness temperature is related to the physical temperature of the object being viewed through the emittance. MSU 54.96 GHz data has also been used to track upper level warming associated with tropopause folds in extratropical cyclones (Velden, 1992).

Dynamical explanations have been put forth in an attempt to place polar lows in the context of tropical cyclone and extratropical cyclone dynamics (Emanuel and Rotunno, 1989; Montgomery and Farrell, 1992). The application of microwave temperature sounding data to detect warming in polar lows will add a third type of storm, the polar low, to the tropical and extratropical cyclones which have been studied with this type of data.

2. Previous satellite sounding observations of polar lows

Satellite observations, primarily from polar orbiting satellites, have played a major role in advancing our knowledge of polar lows. The satellite product most commonly used in polar low research has been infrared window channel imagery. Recently, satellite instruments have become available which can gather more quantitative data about polar lows, such as sea surface wind speed and integrated cloud liquid water (Rasmussen et al., 1993). Satellite observations are critical since the regions where polar lows occur are usually lacking in conventional observations.

Satellite sounding and microwave imaging instruments in particular have shown their utility in extracting information about the polar low and the environment in which it forms (Claud et al., 1993). Satellite temperature retrievals, which employ a combination of infrared and microwave

channels, have been used to detect and track upper level cold pools which can be a precursor to polar low formation (Claud et al., 1992a). The determination of the temperature structure of a mature polar low is difficult due to the small scale of the polar low ($\sim$300 km) as compared to the current resolution of the satellite temperature retrievals ($\sim$100–200 km). Steffensen and Rasmussen (1986) were the first to use satellite derived temperature fields to detect a warm temperature anomaly in both the 850 and 500 mb temperature fields over a polar low. This was done through a temperature retrieval using a combination of infrared channels and MSU data which is referred to as the TIROS Operational Vertical Sounder (TOVS) system. A comparison of TOVS temperature and geopotential retrievals with research aircraft measurements of a polar low was performed by Turner et al. (1992). The satellite temperature soundings using infrared and microwave data revealed the warm core seclusion observed by the aircraft, but the microwave measurements alone did not show an isolated warm area. A problem with performing satellite soundings over a polar low is the presence of clouds, which can cause temperatures retrieved with infrared measurements to be colder than the actual clear sky values. A suitable initial guess for the sounding also needs to be provided, a difficult task for the lowest few hundred millibars of the polar low where strong surface heat fluxes can modify the temperature profile (Turner et al., 1992). Warming was detected over a polar low with satellite temperature sounding by (Claud et al., 1992b). Their temperature retrieval scheme, the Improved Initialization and Inversion (3I) method, indicated warming over the polar low through a product of the retrieval, the mean temperature of the lower stratosphere. This is found from a regression of infrared sounding channels and the 53.74, 54.96, and 57.95 GHz channels of the MSU, and is representative of the mean temperature between 222 and 380 Mb. This warming was probably evidence of a tropopause fold in the upper troposphere, whereas the warming examined in this paper was detected in the lower to middle troposphere.

3. Data sources

The MSU is a 4-channel passive microwave radiometer on board the NOAA series of polar orbiting satellites. For this case study, observations from the satellites NOAA 10 and 11 were used. The MSU senses upwelling radiation at 50.30, 53.74, 54.96, and 57.95 GHz, which are on the wings of an oxygen absorption band centered at 60 GHz. The 50.30, 53.74, and 54.96 frequencies will be referred to as MSU channels 1, 2, and 3 respectively. The brightness temperature is nearly equal to the physical temperature of the emitting oxygen molecules since the emittance of O_2 is close to one. The nadir weighting functions shown in Fig. 1 illustrate the relative contribution of each level to the total radiant energy received for the three lowest MSU frequencies. Fig. 1 shows that the peak of the O_2 emission sensed by channel 2, the frequency of most interest in this study since it responds to the lower and middle levels of the troposphere, comes from near 700 mb, although channel 2 essentially measures the vertically averaged temperature of the entire troposphere (Spencer et al., 1990). Features of the MSU are listed in Table 1. The major issues in using the MSU for the study of polar lows are the resolution of each field-of-view as compared to the horizontal scale of the polar low and the height of the weighting function peak in relationship to the vertical temperature structure of the storm. For polar lows, the MSU horizontal resolution of between 100 and

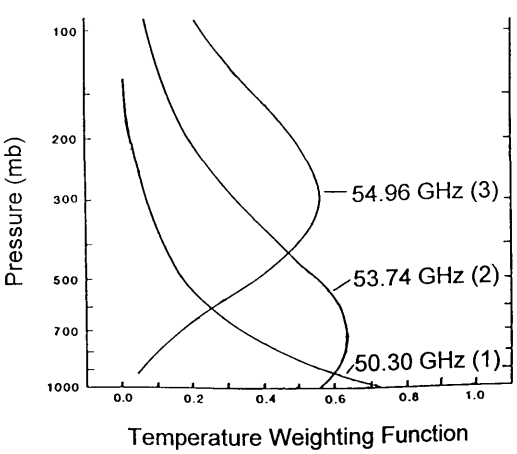

Fig. 1. MSU weighting functions for nadir scan position at 50.30 GHz, 53.74 GHz, and 54.96 GHz, (channels 1, 2, and 3, respectively (indicated in parentheses)). Weighting functions are shown for a surface emittance of 0.5, a typical value of ocean water, (adapted from Grody and Shen (1982)).

Table 1. *Microwave Sounding Unit characteristics*

Parameter	Value
Instrument type:	Dicke radiometer
Channel frequencies:	
channel 1:	50.30 GHz
channel 2:	53.74 GHz
channel 3:	54.96 GHz
channel 4:	57.95 GHz
RF bandwidth:	220 MHz
noise equivalent ΔT_B:	0.3 K
angular resolution:	7.5° (3 dB)
ground field-of-view:	109x109 km at nadir
cross track scan distance:	±1015 km
time per scan:	25.6 s
number of earth views per scan:	11
scan step angle:	9.47°
time between scan steps:	1.84 s

200 km is definitely poor with respect to a typical polar low size of 300 km.

An infrared imaging instrument is also used in this study. This is the Advanced Very High Resolution Radiometer (AVHRR), which is on board the same NOAA satellites as the MSU. The 11 micron channel of the AVHRR is used to provide concurrent views of the clouds associated with the polar low as well as the temperature of the cloud tops. The type of AVHRR data available for this study was Global Area Coverage (GAC) data, which has a nadir resolution of 4 km.

Data from the Special Sensor Microwave/Imager (SSM/I), a multichannel passive microwave radiometer on board the Defense Meteorological Satellite Program satellite F8, is used in this study to infer the wind speed around the polar low. It is also used to detect the edge of the sea ice in the Labrador Sea. The SSM/I has been successfully used to infer physical properties of polar lows such as surface wind speed and integrated water vapor (Claud et al., 1993; Claud et al., 1992a).

4. Data analysis

In this section, channel 2 MSU data will be used to track a warm temperature anomaly over a polar low. This is the first time that this type of data have been examined using T_B anomalies around a polar low. MSU channels 1 and 3 will also be examined in a similar fashion. AVHRR 11 micron imagery will be employed to aid in the assessment of effects other than warming of the air column which could be responsible for the observed channel 2 warm temperature anomalies.

4.1. Synoptic setting and satellite data: 17–18 January 1989

The polar low which is the subject of this case study formed over the Labrador Sea at about 0700 UTC on 17 January 1989 and drifted in an easterly direction until its landfall on the west Greenland coast at about 0300 UTC on 19 January. The area is data sparse with a complete lack of surface and upper air observations over the Labrador Sea. Fig. 2 shows the track of the polar low center on the 17th and 18th as determined from AVHRR imagery. Note the very slow movement of the polar low, only 10 km/hr averaged over its 40 hour lifetime. The ice edge and the location of surface stations at Fredrikshåb and Godthåb are also shown in Fig. 2. The ice boundary along the western portion of the Labrador Sea was deter-

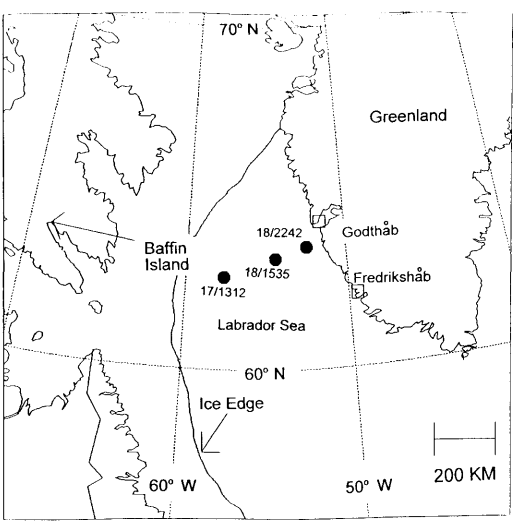

Fig. 2. Location map for the polar low case over the Labrador Sea. The center of the polar low as seen in AVHRR imagery is shown by the solid circles, as well as the time (UTC) on 17, 18 January 1989. The ice edge is shown by the solid line. The surface stations at Fredrikshåb and Godthåb are shown by the hollow squares.

mined from the elevated brightness temperatures seen on the 85 GHz horizontally polarized channel of the SSM/I.

The 500 mb map on 17 January at 1200 UTC is shown in Fig. 3a. The polar low center position, as deduced from AVHRR imagery at 1312 UTC, is also indicated. Note from Fig. 3a that the polar low occurs poleward of the main baroclinic zone, which is to the southeast. Fig. 3a also shows that the 500 mb temperature is −41 °C at the southern tip of Greenland and −42°C over Baffin Island. A 500 mb temperature of less than approximately −42°C appears to be a factor controlling the type of polar low development which occurs (Rasmussen et al., 1993). Fig. 3b shows the surface map at 1200 UTC on 17 January 1989. An area of low pressure was extrapolated to 970 mb over the Labrador Sea. No fronts were indicated with the low. The three hourly surface maps over the next 36 hours hint at the circulation over the Labrador Sea but are not consistent with respect to its location or intensity. Clearly, available synoptic observations were not sufficient to analyze a polar low in this region and must be supplemented by additional observations, such as from satellite.

AVHRR imagery at two times on 17 January (1312 and 1545 UTC) and two times on 18 January (1250 and 1535 UTC) is shown in Fig. 4. Also shown in Fig. 4 are outlines of the isolated warm MSU field-of-views over the polar low as well as the ice edge. The warm MSU field-of-views were defined as those having warmer T_B's than all of the adjacent field-of-views. Note the cold cloud temperatures and spiral cloud pattern which indicate the polar low.

Fig. 5 shows MSU channel 2 T_B imagery at the same four times as in Fig. 4. These were the four times during the two day case study when the position of the MSU scan relative to the polar low was appropriate for analysis. The polar low was required to be located within the seven innermost MSU field-of-views in order to avoid degraded resolution and excessive limb correction, which could yield different results than if the polar low was viewed closer to nadir. This effect has been documented for tropical cyclones by Velden (1989). The field-of-views with isolated warmer T_B's over the polar low are shown by arrows in Fig. 5. There are several features to notice about the sequence of images apart from the warming over the polar low. Note the decrease in resolution of the five MSU field-of-views away from nadir as the outer edge of the swath is approached. The nadir 110 km resolution of the MSU is a factor limiting its utility for the analysis of polar lows. Note also that the elevated terrain of Greenland appears as an area of colder T_B.

The MSU T_B's were limb corrected as well as left in raw form. Limb correction accounts for the apparent change in atmospheric thickness which occurs as the MSU scans away from nadir. Limb corrected radiances are also normalized to unit surface emittance to account for the higher emittance of nonwater surfaces ($\sim$0.9) versus water surfaces ($\sim$0.5), an attempt to make the soundings independent of surface type. Grody (1983) and Koehler (1989) describe the limb correction of MSU data in detail.

The arrows in Fig. 5 indicate the MSU field-of-views with isolated warm T_B's over the polar low. It was not assumed that the position of the isolated warm area was where the polar low was located. Rather, the concurrent AVHRR 11 μ imagery was used to determine the position of the center of the cloud shield associated with the polar low. The tendency of this particular polar low to have an "eye" made this determination straightforward. This case is the first time that MSU channel 2 T_B's over a polar low which are warmer than all the adjacent T_B's have been presented. Turner et al. (1992) detected warming over a polar low through TOVS retrievals but the MSU channel 2 data they present does not show an isolated warm field-of-view over the polar low. Note the persistence of the isolated warming over the two days and the fact that it was detected with the MSU instruments on NOAA 10 and 11. Since MSU channel 2 measurements essentially represent a vertically averaged temperature of the atmosphere, warm column temperature anomalies hydrostatically imply the presence of an accompanying pressure deficit (Velden and Smith, 1983). This is a useful fact for estimating the intensity of a polar low.

In order to better quantify the warming in channel 2 over the polar low, radially averaged T_B values were constructed and subtracted from the isolated warmest T_B over the polar low. This method is similar to the radially averaged T_B values constructed for tropical cyclones (Kidder et al., 1980). The T_B's of the eight field-of-views adjacent to the central area of warming were averaged together to form an environmental mean T_B. Not

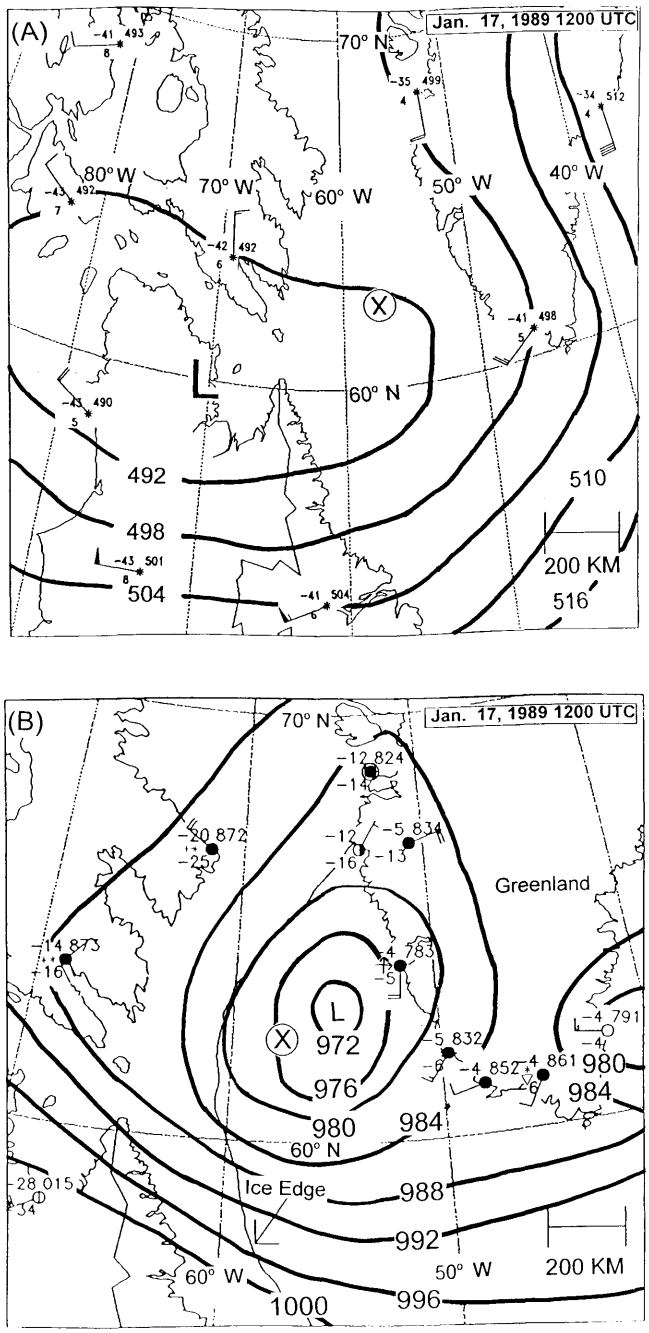

Fig. 3. (A) 500 mb and (B) surface map for 17 January 1989 at 1200 UTC. The 'X' marks the approximate surface position of the polar low. Temperatures are in °C. Wind speeds are shown in m/s (flag = 25 m/s, full barb = 5 m/s, half barb = 2.5 m/s). Surface pressures are contoured at 4 mb intervals, 500 mb heights (× 10 m) are contoured at 60 m intervals. Maps redrawn from data from the National Center for Atmospheric Research (NCAR), Boulder, CO USA.

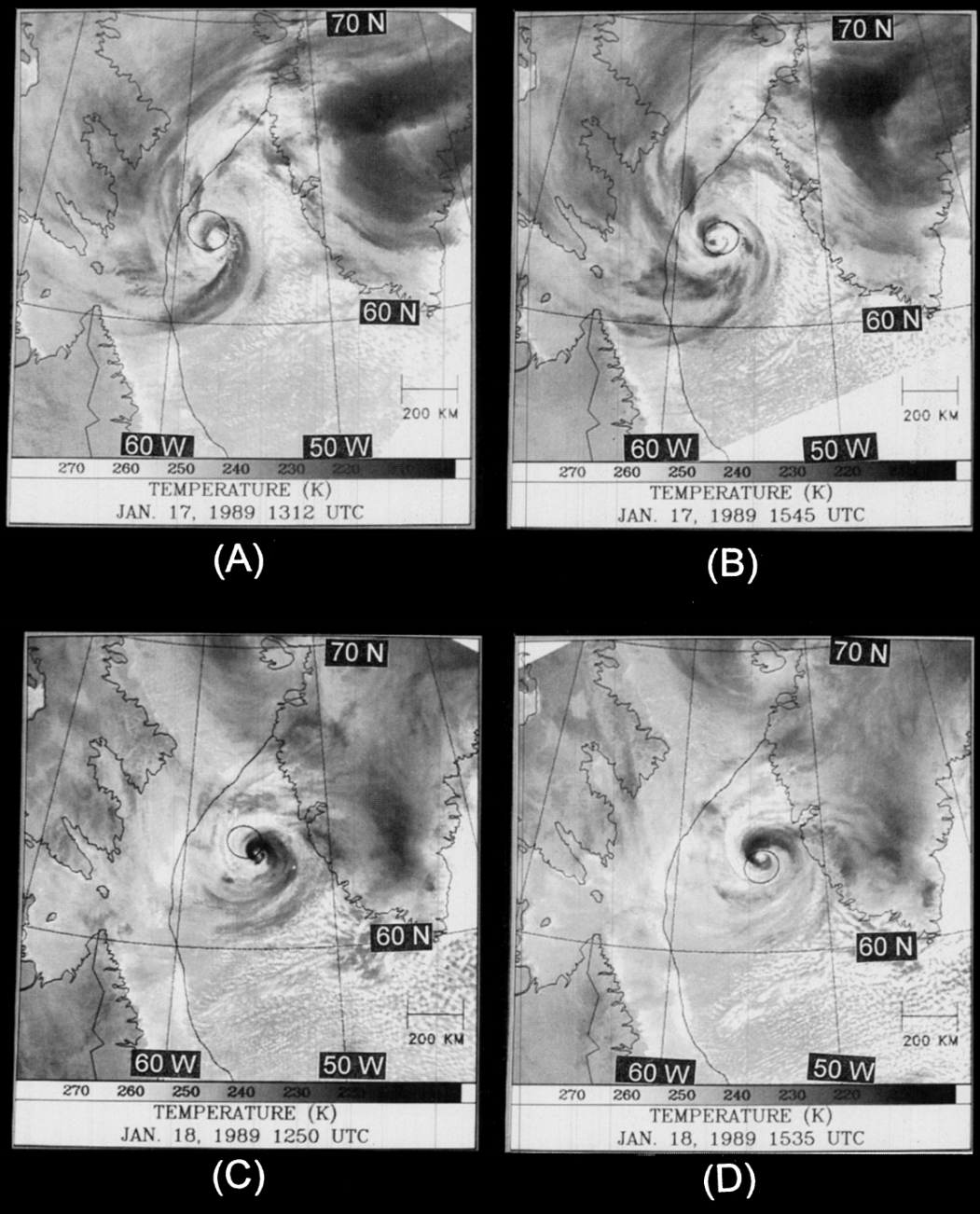

Fig. 4. AVHRR 11 μ imagery at four times (UTC) on 17, 18 January 1989. (A) 17th/1312 (B) 17th/1545 (C) 18th/1250 (D) 18th/1535. The ice edge is indicated as in Fig. 2. The position of the warm isolated MSU 53.74 GHz field-of-view is outlined by an ellipse at each time.

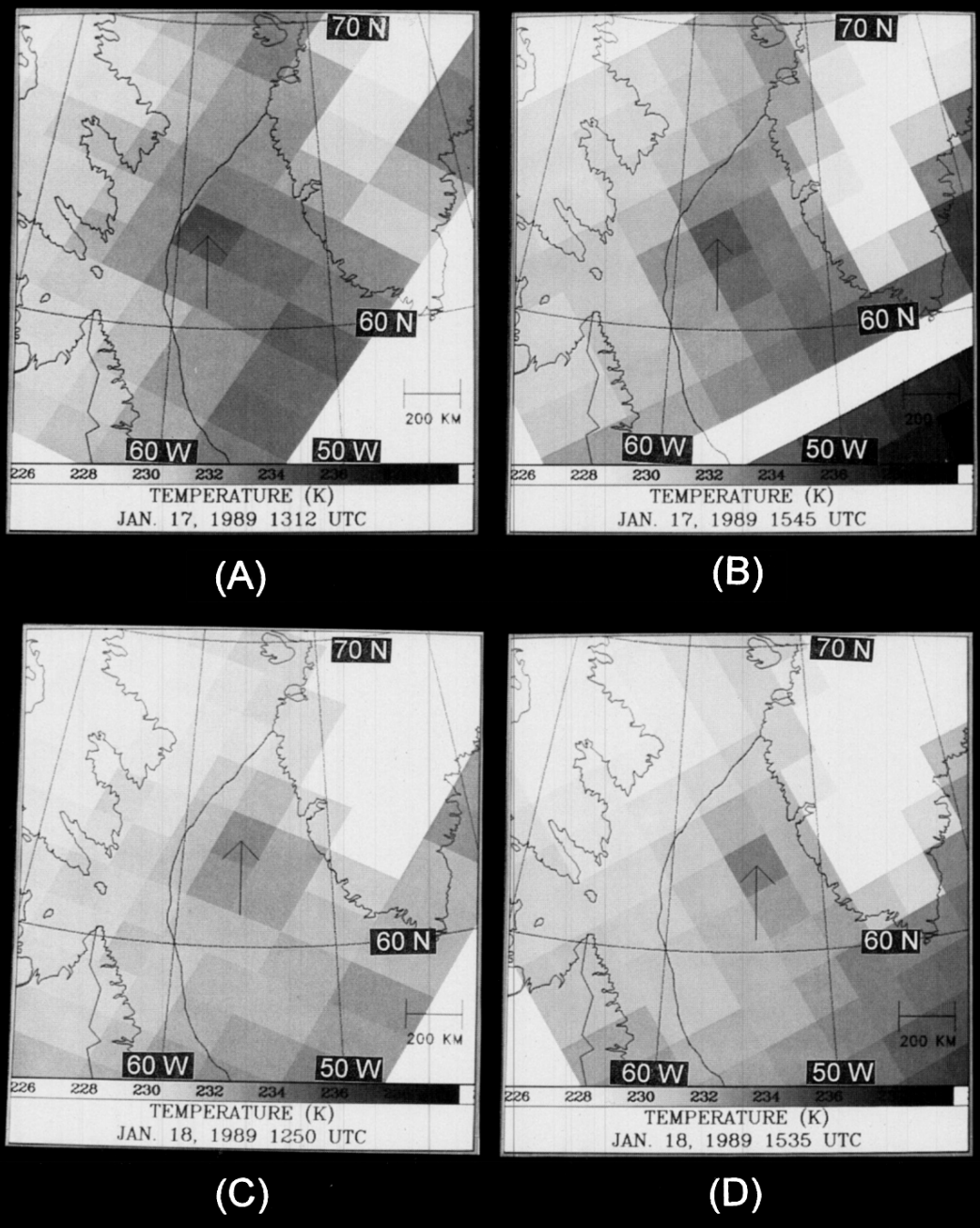

Fig. 5. Limb corrected MSU 53.74 GHz brightness temperatures (K) in imagery form at four times (UTC) on 17, 18 January 1989. (A) 17th/1312 (B) 17th/1545 (C) 18th/1250 (D) 18th/1535. The ice edge is indicated as in Fig. 2. The black line on the 17 January 1545 image is a missing scan line.

all of the 8 adjacent field-of-views were included in the averaging in the following circumstances:

1. the two outermost MSU field-of-views were not employed in the averaging due to poor horizontal resolution and excessive limb correction effects;
2. field-of-views which had any part over land were excluded to avoid returning values which were too cool.

In order to avoid having a cold bias in the environmental mean T_B create a false warm anomaly, the difference between the warmest field-of-view in the channel 2 limb corrected data and the next warmest of the up to eight adjacent field-of-views was also computed. This allowed the T_B difference of adjacent MSU scans to be examined without having excessively cold values skew the radially averaged results.

The results of subtracting the radially averaged T_B from the T_B over the polar low for the four times are given in Table 2. The difference in T_B of the warmest central field-of-view and the next warmest of the up to eight adjacent field-of-views is also given. The positive values of this difference of the next warmest field-of-view show that the warm T_B anomaly over the polar low was not the result of excessively cold environmental T_B values. Anomalies are given for limb corrected as well as non-limb corrected data for channels 2 and 3 along with non-limb corrected data for channel 1 (LC and NLC after the MSU values refer to limb corrected and non-limb corrected values, respectively). The values of the radially averaged anomalies are from 1.4 to 1.9 K in the channel 2 limb corrected data and from 1.6 to 2.5 K in the channel 2 non-limb corrected values. The anomalies in the channel 3 data, with a weighting function peak of about 300 mb, are negligible and within the instrument noise range of 0.3 K. Note that the non-limb corrected channel 1 measurements show both positive and negative temperature anomalies. Channel 1 is less sensitive to O_2 absorption and much more sensitive to clouds and surface variations than channel 2. Changes in the sea surface emittance due to wind stress can also account for changes in the T_B's in channel 1.

Table 3 lists the value of the MSU T_B's over the polar low for the same times as in Table 2. The maximum, minimum, and mean temperatures (K) within the isolated warm MSU field-of-view over the polar low center measured with the AVHRR 11 μ channel are also shown. The temperatures in the "eye" of 274 K on the 17th are near the sea surface temperature in this area and indicate that the center of the polar low was cloud free. The minimum cloud top temperature of 214 K is indicative of clouds which reached the tropopause, at a height of about 8.6 km (300 mb). The height is estimated from the 18 January 1989 1200 UTC sounding from southern Greenland (station location is shown in Fig. 3a), which had a temperature of 214.5 K at 8681 m (300 mb). The mean tem-

Table 2. *MSU brightness temperature anomalies over the polar low for four times on 17 and 18 January 1989*

	Temperature anomaly (K) computed at each time (UTC)			
Quantity	17th, 1312	17th, 1545	18th, 1250	18th, 1535
channel 2 LC	1.6	1.9	1.5	1.9
channel 3 LC	0.2	0.1	0.0	0.0
channel 1 NLC	−6.7	1.1	−0.7	0.4
channel 2 NLC	1.5	2.0	1.4	2.5
channel 3 NLC	0.3	0.1	−0.1	0.2
channel 1 NLC next warmest difference	2.2	0.0	−1.6	−1.2
channel 2 LC next warmest difference	0.8	0.8	0.8	1.0
channel 2 NLC next warmest difference	1.0	0.6	0.6	1.2

Values of the MSU T_B over the polar low minus the next warmest adjacent T_B are also given. LC and NLC after the values refer to limb corrected and non-limb corrected values, respectively. Positive MSU anomaly values indicate polar low warmer than environment. All values are in K.

Table 3. *MSU brightness temperatures and AVHRR 11 μ temperatures over the polar low for four times on 17 and 18 January 1989*

	Temperature (K) at each time (UTC)			
Quantity	17th, 1312	17th, 1545	18th, 1250	18th, 1535
channel 2 LC	234.6	234.8	233.6	233.4
channel 3 LC	214.4	214.2	213.2	213.6
channel 1 NLC	224.8	221.6	220.0	222.0
channel 2 NLC	231.0	232.6	231.4	231.2
channel 3 NLC	212.4	213.2	212.2	212.4
AVHRR 11 μ minimum	224.8	224.4	217.5	214.1
AVHRR 11 μ maximum	274.0	274.3	271.8	273.4
AVHRR 11 μ mean	246.9	252.6	246.7	247.5

LC and NLC after the MSU values refer to limb corrected and non-limb corrected values, respectively. The warmest, coldest and mean AVHRR 11 μ temperatures within the elliptical MSU field-of-view over the polar low center are also given. All values are in K.

peratures were computed from the pixels within the MSU field-of-view and are clustered around 247 K.

There are several features of Tables 2 and 3 which are important for this study. The channel 2 temperature anomalies in Table 2 are positive for both the raw and limb corrected data. This shows that T_B anomalies over the polar low were not an artifact of the limb correction procedure. The difference of the channel 2 T_B over the polar low minus any of the eight adjacent T_B's is always positive, indicating the isolated nature of the warming over the polar low. The limb corrected channel 2 T_B in Table 3 decreases by a little over 1 K between 17 and 18 January, but the warm T_B anomaly in Table 2 continues. This may indicate the movement of an upper level cold pool. 500 mb temperatures at the Baffin Island rawinsonde station (Fig. 3a) decreased from −42°C at 1200 UTC on 17 January to −45°C at 1200 UTC on the 18 January. The limb corrected channel 3 T_B measurements in Table 3 show a slight decrease between the 17th and 18th. The non-limb corrected measurements in the MSU channel 1 are more variable over time than any of the other MSU channels, showing both positive and negative temperature anomalies over the polar low. The fact that the channel 1 measurements do not a show a consistent warm anomaly over the polar low is evidence that cloud and surface effects were not responsible for the warming in channel 2, since channel 1 is much more sensitive to these effects.

4.2. *Non-O_2 effects on the 53.74 GHz measurements*

Table 2 shows that for 4 NOAA satellite passes over a period of 2 days, the MSU 53.74 GHz channel (channel 2) revealed isolated warmer T_B's over a polar low. The possibility that effects other than O_2 emission could be responsible for the observed warming in channel 2 will now be examined.

The fact that MSU T_B anomalies over a polar low were detected in the channel 2 rather than in channel 3 makes the results more susceptible to non-O_2 effects since the channel 2 weighting function has more contribution from the surface and lower troposphere (Fig. 1). The advantage of using channel 3 to sense warm temperature anomalies, as has been done with this channel in the case of tropical and extratropical cyclones (Velden, 1992; Velden, 1989), is that the effect of ice in deep convective clouds is to *decrease* or leave unchanged any warm T_B anomaly which is due to actual warming in the air column. Therefore, no false warm anomalies due to non-O_2 effects are produced in the channel 3 data. Due to the lower vertical extent of polar lows, MSU channel 2 data must be used to detect the temperature anomaly. In tropical cyclone studies, the channel 2 T_B is reduced from clear sky values due to scattering from ice in very deep convection. Whether clouds over the ocean will result in warming or cooling for measurements near 53.74 GHz depends on the liquid water content of the cloud and the height of the cloud

Table 4. *Sensitivity of MSU 53.74 GHz measurements to various geophysical parameters (after Spencer et al. (1990))*

Geophysical parameter	MSU 53.74 GHz T_B sensitivity (K)
oxygen emission by the atmosphere:	0.92° per +1° (land) 0.96° per +1° (ocean)
sea surface temperature	0.036° per +1°
sea surface wind speed	0.01° per 1 m/s incr. in wind speed
water vapor (ocean)	+0.02° per 20% in polar air mass
cirrus clouds	0° (thin cirrus), −1° (thunderstorm)
cloud water (ocean):	100% increase in coverage or amount
low clouds (900–950 mb)	+0.1° to +0.2°
middle clouds (600–700 mb)	−0.1°

(Rosenkranz et al., 1972). Low clouds will tend to increase T_B's due to emission from liquid water while higher clouds will decrease T_B's due to depletion of upwelling radiation by ice particles. Microwave measurements at the MSU frequencies are much less sensitive to emission from ice clouds than from water clouds (Grody and Shen, 1982; Kidder et al., 1978).

Spencer et al. (1990) studied the sensitivity of MSU channel 2 measurements to non-O_2 effects as part of an effort to measure global tropospheric temperature. The sensitivity of channel 2 T_B to various geophysical parameters is given in Table 4. They conclude that cumuliform clouds over water which extend from 950 to 650 mb will have essentially no effect on MSU 53.74 GHz measurements, while cumuliform clouds above about 650 mb will have a cooling effect. For this case, a comparison of AVHRR measurements of cloud top temperature with the temperature sounding at Baffin Island yields average cloud tops over the polar low of from 800 to about 650 mb, with highest cloud tops in the MSU field-of-view from 500 to 300 mb. This is near or above the level where emission by liquid water will be balanced out or even overshadowed by scattering and T_B depression from ice particles. At the 500 mb level, temperatures are colder than −40°C, allowing homogeneous nucleation of water into ice particles. Airborne radar observations of a polar low (Shapiro et al., 1987) indicated that the convective precipitation was confined to within 3 km of the surface, or pressures higher than about 700 mb in this case.

The sensitivities in Table 4 have been used to construct Table 5, which shows some possible upper bounds to non-O_2 warming observed in MSU channel 2 data. The doubling in water vapor content is assumed to be reasonable based on the measurements of Shapiro et al. (1987). It is likely that some of these effects will be correlated, for instance strong winds are likely to occur in a cloudy area in a storm. Note that by not allowing for any cooling effects, the maximum T_B increase at 53.74 GHz due non-O_2 effects is about +1°C. We have not accounted for any reduction in the T_B anomaly which may occur through spreading a

Table 5. *Possible increases in MSU 53.74 GHz brightness temperature over a polar low due to non-O_2 effects using the sensitivities in Table 4*

Parameter	Polar low vs. ambient	MSU 53.74 GHz T_B increase (K)
sea surface temperature	3 K higher	0.1
sea surface wind speed	20 m/s higher	0.2
water vapor	100% increase	0.1
cloud liquid water	100% increase	0.2
instrument noise		0.3
	total possible increase: ~1.0	

warm temperature anomaly over two or more MSU field-of-views. This would mean that a part of the central warming could be spread into one or more of the eight adjacent MSU field-of-views. The radially averaged channel 2 warm anomalies in Table 2 are always greater than +1°C and range up to 1.9°C. The differences of the next warmest MSU channel 2 field-of-views are also all near 1°C. This is evidence that the MSU measurements for this particular case reveal warming in the air column with this polar low. This does not mean that all polar lows are associated with warming which can be detected with the MSU. Other polar lows cases examined from the Labrador Sea region in 1989 (11 January (Rasmussen et al., 1993), 20 March) did not show isolated warming in the MSU data like the 17–18 January case.

4.3. *Surface observations*

Evidence of the circulation and weather associated with the polar low was seen in surface observations from two stations along the west Greenland coast as the polar low crossed the coast between these stations at about 0300 UTC on 19 January 1989 (Fig. 2). Station plots at three hour intervals for Fredrikshåb and Godthåb for the 24 h period between 1200 UTC on 18 January and 1200 UTC on 19 January are shown in Fig. 6. Note the rise in surface temperature (from −6°C to −3°C and back to −6°C) which occurs at Fredrikshåb between 2100 UTC on the 18th to 1200 UTC on the 19th. At 2100 UTC on the 18th, Fredrikshåb reported a pressure of 991.1 mb while an offshore ship report had a pressure of 988.2 mb with heavy snow and southwesterly winds at 20 m/s.

Evidence that a surface circulation was associated with the polar low when it was over the Labrador Sea is provided by surface wind speeds retrieved with the SSM/I. The wind speeds were retrieved using a statistical algorithm (Goodberlet et al., 1989), in conjunction with the accuracy flagging and moving average revisions suggested by Petty and Katsaros (1990). The wind speeds retrieved with this method have a 2 m/s standard deviation when compared with surface wind

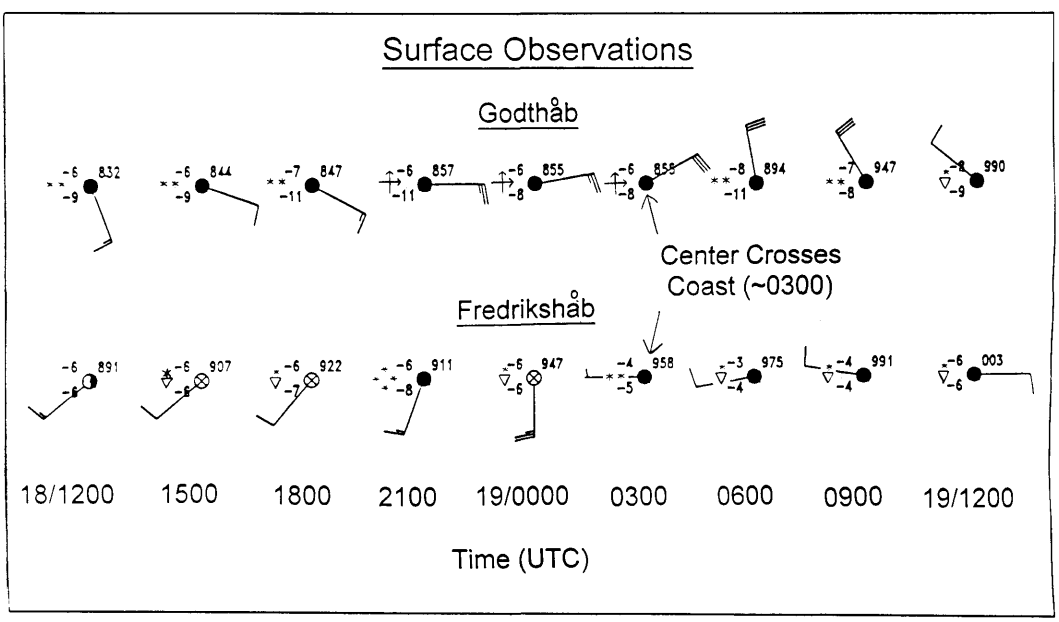

Fig. 6. Three hourly station plots from Fredrikshåb and Godthåb for the period from 1200 UTC on 18 January 1989 through 1200 UTC on 19 January 1989. Wind speeds are in m/s (full barb = 5 m/s, half barb = 2.5 m/s), temperatures are in °C and pressures are in mb. Note the maximum in temperature at Fredrikshåb at 0600 UTC on the 19th. The polar low crossed the Greenland coast between these two stations at about 0300 UTC on 19 January (Fig. 2).

speeds for speeds below about 16 m/s. The horizontal resolution of the surface wind speeds is about 40 km. Fig. 7 shows SSM/I surface wind speed retrievals at 0829 UTC on 18 January. The values are shaded at 2 m/s intervals. The approximate polar low position is indicated by an arrow. Wind speeds were not retrieved in the crescent shaped black area over the polar low due to precipitation effects (accuracy flag "1" of Goodberlet et al., 1989). Pixels adjacent to those flagged with accuracy flag "1" were also flagged themselves in accordance with Petty and Katsaros (1990), which has the effect of expanding the flagged region. Note the retrieved wind speeds of approximately 20 m/s along the western side of the polar low, and wind speeds of less than 10 m/s between the polar low and the Greenland coast.

The minimum difference of the SSM/I 37 GHz vertically polarized minus the 37 GHz horizontally polarized channel was 40 K, which was in an area in which wind speeds were not retrieved due to accuracy flagging. Smaller values of this difference indicate increasing depolarization of the upwelling radiation due to precipitation. For $T_{37v} - T_{37h} =$ 40 K, wind speeds retrieved with this algorithm can be expected to have a standard deviation of about 4 m/s and similar positive bias. This indicates that the precipitation over the central area of the polar low did not degrade the surface wind speed retrievals significantly. This shows an advantage of using the SSM/I to retrieve wind speeds in polar lows as compared to observing storms in more temperate latitudes. The lower liquid water and water vapor content of the polar

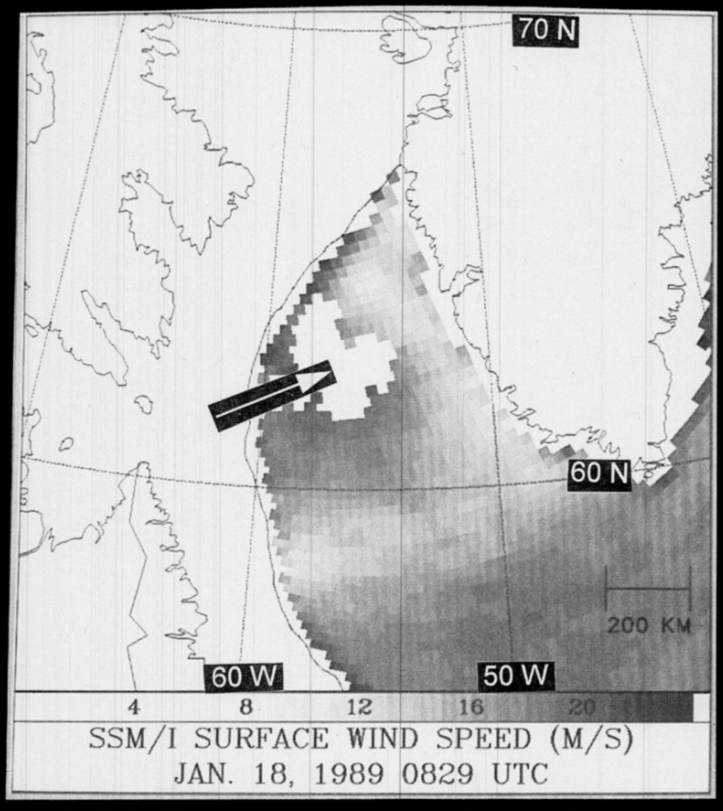

Fig. 7. SSM/I surface wind speeds shaded at 2 m/s intervals for 18 January 1989 at 0829 UTC. Polar low position is indicated by an arrow. Winds are not retrieved in the crescent shaped black area near the polar low due to accuracy flagging.

atmosphere allows for less obstruction of the surface wind speed signal. Using a revision (Goodberlet and Swift, 1992) of the original SSM/I wind speed algorithm which is valid in precipitating areas where $T_{37v} - T_{37h} > 35$ K, wind speeds of up to 24 m/s were retrieved over the polar low center at 0829 UTC on 18 January with no pixels flagged for accuracy.

5. Conclusions

A polar low over the Labrador Sea was observed to possess an isolated warm T_B anomaly in MSU channel 2 measurements on four satellite passes over a two day period. The magnitude of the warming was from between 1 and 2 K of T_B. Such warming is expected for certain types of polar lows which become warm core systems. The isolated warming was only observed in MSU channel 2 data, indicating that the warming was strongest in the middle troposphere. Wind speeds from the SSM/I indicated a surface circulation of about 20 m/s, and surface observations from the Greenland coast also indicated a surface circulation with the polar low.

The possibility that effects other than warming of the air column in the polar low were responsible for the measured T_B anomaly in the polar low was investigated. Clouds, precipitation, and increases in surface emittance can weakly increase the channel 2 T_B when viewing over a water background. Most studies utilizing MSU data to look at temperature anomalies over storms have utilized MSU channel 3 where non-O_2 warming is negligible. In this polar low case, there are several indications that the overall effect of non-O_2 impacts on the channel 2 warm T_B anomaly were neutral or even negative. MSU channel 1, which is much more sensitive to non-O_2 warming effects, did not show a concurrent positive T_B anomaly with the channel 2 measurements. Cloud top temperatures over the polar low derived from infrared measurements were as low as 214 K, and averaged near 247 K. The cloud tops at these temperatures would consist predominantly of ice and decrease or have no effect on 53.74 GHz satellite T_B measurements. Ignoring the likely cooling effects of the clouds over the polar low, the maximum possible non-O_2 warming in the channel 2 data was estimated to be 1 K. Radially averaged channel 2 temperature anomalies ranged up to 2 K, indicating that some warming of the air column was detected in the MSU data.

All of the difficulties encountered in applying MSU temperature measurements to tropical cyclone warm core estimation (Velden, 1989) are also present in applying the measurements to polar lows. Horizontal and vertical resolution limitations of the MSU are even more troublesome in polar low applications due to the smaller horizontal and vertical scale of the polar low. Proximity of the polar low to land or ice and strong ambient temperature gradients makes it more difficult to radially average temperatures around the polar low to get an environmental temperature value. On the positive side, polar orbiting satellites which carry microwave instruments sample the polar areas more frequently than areas further equatorward.

The detectability of atmospheric warming over polar lows could have several implications for our understanding of polar lows. The source of the low-level warm core observed in many polar low case studies is not always clear. Seclusion of warm air or heating through convection and surface fluxes have been suggested as possible sources. Satellite measurements could be used to determine if atmospheric warming is always associated with, for instance, deep convection. The development of a warm core in a polar low is associated with an intensification of the surface circulation of the storm (Rasmussen et al., 1993). Perhaps satellite monitoring of warming in a polar low could be used to determine whether this transition has occurred. It may be possible to develop forecasting guidelines relating satellite observed warming to surface parameters such as wind speed or pressure deficit. Given the scarcity of conventional data in regions where polar lows often occur, optimal use of satellite data is essential in analysis and forecasting of these storms.

More data needs to be gathered on the effects of the clouds and precipitation found in a mature polar low on microwave measurements. This falls in with a general need for more field observations of polar lows. Cloud properties observed in a polar low could be input to radiative transfer models to assess their effect on microwave measurements. The impact of these effects could then reduced in the temperature sounding data, allowing a more

accurate determination of the atmospheric thermal structure. Multichannel inversion of the satellite data could be done to retrieve vertical temperature profiles. The next generation of the MSU, the Advanced Microwave Sounding Unit (AMSU; scheduled for launch in 1996 on NOAA-K), will have about twice the horizontal resolution of the MSU, more channels, and better vertical resolution. It will also have channels that are at window frequencies, which will allow better consideration of cloud effects. The AMSU will be an exciting platform on which to continue work on satellite monitoring of polar lows.

6. Acknowledgments

This work was supported during the thesis stage by the National Oceanic and Atmospheric Administration under NOAA grant 90RAH00077. Thanks are extended to Erik Rasmussen and Michael Montgomery for many valuable discussions about polar lows, Andrew Jones for use of the PORTAL system to process the satellite data and advice on the manuscript, Deborah Molenar for assistance in obtaining the data, and Loretta Wilson and Don Reinke for help throughout the course of this work.

REFERENCES

Businger, S. and Reed, R. J. 1989. Polar lows. In P. F. Twitchell, E. A. Rasmussen and K. L. Davidson (eds.): *Polar and arctic lows*. A. Deepak Publishing, Hampton, Virginia, 3–45.

Businger, S. and Baik, J.-J. 1991. An arctic hurricane over the Bering Sea. *Mon. Wea. Rev.* **119**, 2293-2322.

Claud, C., Katsaros, K. B., Petty, G. W., Chedin, A. and Scott, N. A. 1992a. A cold air outbreak over the Norwegian Sea observed with the TIROS-N Operational Vertical Sounder (TOVS) and the Special Sensor Microwave/Imager (SSM/I). *Tellus* **44A**, 100–118.

Claud, C., Scott, N. A. and Chedin, A. 1992b. Use of TOVS observations for the study of polar and arctic lows. *Intl. J. Remote Sensing* **13**, 129–139.

Claud, C., Mognard, N. M., Katsaros, K. B., Chedin, A. and Scott, N. A. 1993. Satellite observations of a polar low over the Norwegian Sea with the Special Sensor Microwave Imager, Geosat, and TIROS-N Operational Vertical Sounder. *J. Geophys. Res.* **98**, 14487–14506.

Douglas, M. W., Fedor, L. S. and Shapiro, M. A. 1991. Polar low structure over the Northern Gulf of Alaska based on research aircraft observations. *Mon. Wea. Rev.* **119**, 32–54.

Emanuel, K. A. and Rotunno, R. 1989. Polar lows as arctic hurricanes. *Tellus* **41A**, 1–17.

Forbes, G. S. and Lottes, W. D. 1985. Classification of mesoscale vortices in polar airstreams and the influence of the large-scale environment on their evolutions. *Tellus* **37A**, 132–155.

Forsythe, J. M. 1993. *Satellite microwave observations of polar lows. Dept. of Atm. Sci. Paper no. 525.* Colorado State University, Fort Collins, Colorado, USA 152 pp.

Goodberlet, M. A. and Swift, C. T. 1992. Improved retrievals from the DMSP wind speed algorithm under adverse weather conditions. *IEEE Trans. Geosci. and Remote Sensing*. **30**, 1076–1077.

Goodberlet, M. A., Swift, C. T. and Wilkerson, J. C. 1989. Remote sensing of ocean surface winds with the Special Sensor Microwave/Imager. *J. Geophys. Res.* **94**, 14547–14555.

Grody, N. C. 1983. Severe storm observations using the Microwave Sounding Unit. *J. Climate and Applied Meteor.* **22**, 609–625.

Grody, N. C. and Shen, W. C. 1982. *Observations of Hurricane David (1979) using the Microwave Sounding Unit.* NOAA Tech. Rep. NESS 88, 52 pp.

Kidder, S. Q., Gray, W. M. and Vonder Haar, T. H. 1978. Estimating tropical cyclone central pressure and outer winds from satellite microwave data. *Mon. Wea. Rev.* **106**, 1458–1464.

Kidder, S. Q., Gray, W. M. and Vonder Haar, T. H. 1980. Tropical cyclone outer winds derived from satellite microwave sounder data. *Mon. Wea. Rev.* **108**, 144–152.

Koehler, T. L. 1989. Limb correction effects on TIROS-N Microwave Sounding Unit observations. *J. Applied. Meteor.* **28**, 807–817.

Montgomery, M. T. and Farrell, B. F. 1992. Polar low dynamics. *J. Atmos. Sci.* **49**, 2484–2505.

Nordeng, T. E. and Rasmussen, E. A. 1992. A most beautiful polar low. A case study of a polar low in the Bear Island region. *Tellus* **44A**, 81–99.

Petty, G. W. and Katsaros, K. B. 1990. New geophysical algorithms for the Special Sensor Microwave Imager. Preprints. *5th. Conf. on Satellite meteorology and oceanography.* London, England. Amer. Meteor. Soc., Boston, Mass. 247–251.

Rasmussen, E. 1985. A polar low development over the Barents Sea. *Tellus* **37A**, 407–418.

Rasmussen, E. 1989. A comparative study of tropical cyclones and polar lows. In P. F. Twitchell, E. A. Rasmussen and K. L. Davidson (eds.): *Polar and arctic lows*. A. Deepak Publishing, Hampton, Virginia, 47–80.

Rasmussen, E. A and Purdom, J. F. W. 1992. Investigations of a polar low using geostationary satellite imagery. Preprints. *5th. Conf. on Satellite meteorology and oceanography*. Atlanta, Georgia. Amer. Meteor. Soc., Boston, 120–122.

Rasmussen, E., Turner, J. and Twitchell, P. F. 1993. Report of a workshop on applications of new forms of satellite data in polar low research. *Bull. Amer. Meteor. Soc.* **74**, 1057–1073.

Rosenkranz, P. W., Barath, F. T., Blinn III, J. C., Johnston, E. J., Lenoir, W. B., Staelin, D. H. and Waters, J. W. 1972. Microwave radiometric measurements of atmospheric temperature and water from an aircraft. *J. Geophys. Res.* **77**, 5833–5844.

Shapiro, M. A., Fedor, L. S. and Hampel, T. 1987. Research aircraft measurements of a polar low over the Norwegian Sea. *Tellus* **39A**, 272–306.

Spencer, R. W., Christy, J. R. and Grody, N. C. 1990. Global atmospheric temperature monitoring with satellite microwave measurements: methods and results 1979–1984. *J. Climate* **3**, 1111–1128.

Steffensen, M. and Rasmussen, E. 1986. *An investigation of the use of TOVS data in polar low research*. Tech. Rep. No. 25. The Norwegian Meteorological Institute, Oslo, Norway 45 pp.

Turner, J., Lachlan-Cope, T. A. and Moore, J. C. 1992. A comparison of satellite sounding data and aircraft measurements within a mature polar low. *Tellus* **44A**, 119–132.

Van Delden, A. 1989. On the deepening and filling of balanced cyclones by diabatic heating. *Meteorol. Atmos. Phys.* **41**, 127–145.

Velden, C. S. 1992. Satellite-based microwave observations of tropopause-level thermal anomalies: qualitative applications in extratropical cyclone events. *Wea. Forecasting*. **7**, 669–682.

Velden, C. S. 1989. Observational analyses of North Atlantic tropical cyclones from NOAA polar-orbiting satellite microwave data. *J. Applied Meteor.* **28**, 59–70.

Velden, C. S. and Smith, W. L. 1983. Monitoring tropical cyclone evolution with NOAA satellite microwave observations. *J. Clim. Applied Meteor.* **22**, 714–724.

Velden, C. S., Goodman, B. M. and Merrill, R. T. 1991. Western North Pacific tropical cyclone intensity estimation from NOAA polar-orbiting satellite microwave data. *Mon. Wea. Rev.* **119**, 159–168.